J Electroceram (2007) 18:183–188
DOI 10.1007/s10832-007-9022-9

Solubility of Ni in $BaTiO_3$ during co-firing

Yung-Ching Huang · Wei-Hsing Tuan

Received: 29 November 2005 / Accepted: 21 December 2006 / Published online: 27 February 2007

Abstract Nickel is now frequently used as internal electrodes for multilayer ceramic capacitors (MLCC). In order to evaluate the effect of the presence of metallic Ni on the properties of $BaTiO_3$-based dielectrics, nano-sized Ni particles are mixed thoroughly with $BaTiO_3$ powder and subsequently sintered at 1,330 °C in nitrogen. The oxygen partial pressure in the nitrogen is slightly higher than the equilibrium oxygen partial pressure for the Ni→NiO reaction. Under such a condition, an upper limit of 5,400± 540 ppm for the solubility of Ni in $BaTiO_3$ is detected. The Ni solute acts as an acceptor to $BaTiO_3$, and its presence increases the reduction resistance of $BaTiO_3$ significantly.

Keywords Dielectric · Solubility · Barium titanate · Nickel

1 Introduction

Nickel is now frequently used as inner electrodes for multilayer ceramic capacitors (MLCC). Due to the economic feasibility of nickel, it is now possible to manufacture high capacitance MLCC. For example, the capacitance of a 700-layer Ni-MLCC (with the thickness of the dielectric layer as small as 2 μm) can reach a value as high as 100 μF [1]. In such MLCC, the nickel electrodes are packed closely together. With this kind of geometry arrangement, the following issues are then raised:

1. What is the solubility of Ni in $BaTiO_3$-based dielectrics?
2. If Ni is soluble in the dielectrics, how far away can it diffuse?
3. If Ni dose dissolve into $BaTiO_3$, what is the effect of Ni solute on the dielectric properties?

Despite the continuous trend of reducing the dielectric thickness in electronic devices, to the surprise of the present authors, the above issues attract little attention. The available data on the solubility and diffusion of Ni in $BaTiO_3$-based dielectrics are summarized in Table 1 [2–7]. From the Table, the limited data suggest many inconsistencies. One previous study suggested that the solubility of Ni in $BaTiO_3$ is a function of oxygen partial pressure in the sintering atmosphere [3]. Though the solubility of Ni in $BaTiO_3$ is relatively low, the diffusion distance is approaching the same order of the dielectric thickness [7], which is typically around 5 μm in present-day electronics.

In order to investigate the above three issues, nano-sized Ni particles are mixed thoroughly with a $BaTiO_3$ powder. The solubility of Ni in $BaTiO_3$ is then measured by two independent measurement techniques; X-ray diffractometry (XRD) and electron probe micro-analysis (EPMA) techniques. The diffusion distance is also estimated. The dielectric properties of the Ni-doped $BaTiO_3$ are measured.

2 Experimental

Barium titanate powder (trade name: NEB, Ferro Co., USA) and various amounts of nickel nitrate (ACROS Organics Co., USA) were tumble-milled together in ethyl alcohol for 4 h. The Ba/Ti ratio of the $BaTiO_3$ powder is 1.000±0.002, as reported by the manufacturer. The grinding media used were zirconia balls. The slurry of the powder mixture was dried in a rotary evaporator. The dried mixture lumps were then crushed and sieved. The resultant powder was calcined in air at 500 °C for 2 h to remove NO_x, and then pressed uniaxially at 25 MPa into disc

Y.-C. Huang · W.-H. Tuan (✉)
Department of Materials Science and Engineering,
National Taiwan University,
Taipei 106, Taiwan
e-mail: tuan@ccms.ntu.edu.tw

Table 1 Reported values on solubility and diffusion of Ni in $BaTiO_3$.

Related issues	Reported values/heat treatment conditions	Technique employed	References
Solubility of Ni in Ti-excess $BaTiO_3$	4,000 ppm/1,350–1,420°C, air	Curie temperature	[2]
Solubility of NiO in $(BaTiO_3)_{0.865}(CaZrO_3)_{0.135}$	Nil/1,350°C, $P_{O2}=10^{-6}$ Pa	Curie temperature	[3]
Solubility of NiO in $(BaTiO_3)_{0.865}(CaZrO_3)_{0.135}$	3,000 ppm/1,350°C, $P_{O2}=10^{-2}$ Pa	Curie temperature	[3]
Solubility of Ni in Ti-excess $BaTiO_3$	6,400 ppm/1,400°C, air	Magnetic susceptibility	[4]
Solubility of Ni in $BaTiO_3$	8,000 ppm/not available	Not available	[5]
Solubility of Ni in Ti-excess $BaTiO_3$	6,400 ppm/1,290°C, air	Sintering & grain growth	[6]
Diffusion distance of Ni in a Y5V composition $(Ba_m(Zr_xTi_{1-x})O_3)$	0.5 μm/1,250°C/2 h in $P_{O2} = 10^{-5} - 10^{-7}$ Pa	TEM-EDX	[7]

specimens. The dimensions of the discs were 10 mm in diameter and about 3 mm in thickness. The disc specimens were fired at 800 °C for 2 h in a 95%N_2/5%H_2 atmosphere to reduce the NiO contained within the specimen into Ni. After these preparations, fine Ni particles would be in close contact with the $BaTiO_3$ particles. The morphology of the particles was observed with transmission electron microscopy (TEM). The amount of nickel after the reduction procedure was determined by inductively couple plasma-atomic emission spectroscopy (ICP-AES, S-35, Kontron Co., Germany). For comparison purpose, several $BaTiO_3$ green compacts without the pre-reduction treatment at 800 °C were also prepared.

Sintering was performed at 1,330 °C for 2 h with continuous supply of N_2 inside a tube furnace. The heating and cooling rates were 3 °C/min. The oxygen partial pressure in the sintering atmosphere was monitored with a zirconia oxygen sensor. The final density of the specimens was determined by the water displacement method. The specimens were ground and polished with SiC and Al_2O_3 particles, respectively. Etching with a dilute solution of HCl and HF revealed the grain boundary of the polished specimens. The microstructure was observed under a field-emission scanning electron microscopy (FE-SEM, LEO 1530, Philips, The Netherlands).

Two techniques were used to determine the solubility of Ni in $BaTiO_3$. The first technique employed an X-ray diffractometer (XRD, Model Philips PW 1830, Philips, The Netherlands) operating at 30 kV and 20 mA. A slow scanning rate with the step size of 0.01° and 2 second per step was used to determine the lattice parameters, c and a. Three specimens were examined for any particular Ni-$BaTiO_3$ composition.

The second technique employed an electron probe micro-analyzer incorporated with wavelength dispersive spectroscopy (EPMA-WDS, JEOL JAX-8600SX, Japan) operating at 15 kV and 10 μA. This operation condition would result in an electron probe with a spot size of 1.5 μm. The detection limit of this technique was, depending on the type of element investigated, lower than 100 ppm. Polished specimens doped with 0.70, 3.5 and 6.8 mol% Ni were analyzed by the EPMA-WDS techniques; an undoped $BaTiO_3$ specimen acted as a reference sample. Since the Ni particles were mixed thoroughly with the $BaTiO_3$ particles, many Ni inclusions were observed within the $BaTiO_3$ matrix. When a Ni inclusion within the $BaTiO_3$ matrix was located on the polished surface by the EPMA mapping analysis, the specimen was analyzed along a straight line from this discovered Ni inclusion in 1-μm steps; around 20 points (i.e. a distance of 20 μm) were measured. Data from five different lines for each composition were obtained from the polished surface. Detailed procedures of using EPMA-WDS to determine minute solubility can be found in the existing literature [8].

The dielectric properties of the specimens were measured by a LCZ meter (2330 A, NF Electronic Instruments, Japan) with a detection signal of ±1 V at 1 kHz. Silver pastes were applied as the external electrodes.

3 Results

Figure 1 shows the XRD patterns for a 32 mol% Ni-$BaTiO_3$ after calcination at 500 °C in air, reduction at 800 °C in H_2/

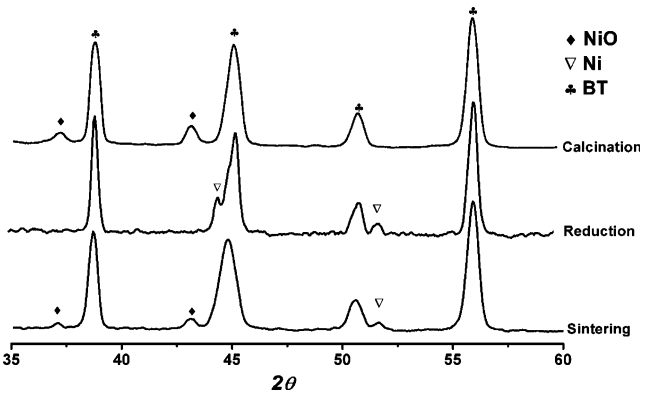

Fig. 1 XRD patterns for $BaTiO_3/Ni(NO_3)_2$ powder mixture after calcination at 500°C for 2 h in air, reduction at 800°C for 2 h in N_2/H_2, and sintering at 1,330°C for 2 h in N_2; the Ni amount is 32 mol%

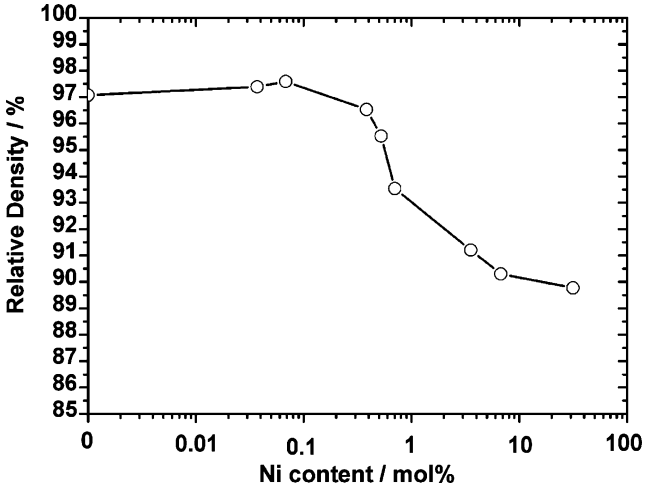

Fig. 2 Relative density of sintered Ni-doped $BaTiO_3$ specimens as function of Ni content

N_2 mixture, and then sintering at 1,330°C in N_2. During calcination, nickel nitrate was decomposed into nickel oxide, which was subsequently reduced to nickel at 800°C. In Fig. 1, the amount of Ni, determined by ICP-AES technique, is 8.5 wt%, which corresponds to 32 mol% Ni. For other Ni-doped $BaTiO_3$ specimens prepared for this study, their Ni contents determined by ICP-AES vary from 370 ppm to 32 mol%.

Both Ni and NiO are found in the specimens after sintering at 1,330°C for 2 h in nitrogen. The oxygen partial pressure in the nitrogen is 1 Pa, as determined by the zirconia oxygen sensor located above the specimen. By using Scherer's relationship [9], the size of the resulting Ni particles in the reduced powders is 70 nm. This value is also confirmed by using the TEM technique.

Figure 2 shows the relative density of the Ni-doped $BaTiO_3$ specimens after sintering. Similar to the effect of NiO on the densification of $BaTiO_3$ [6], the addition of metallic Ni particles decreases the density of the specimen. Figure 3 shows a typical micrograph of the sintered 32 mol% Ni-doped $BaTiO_3$ specimen. Fine Ni particles mainly locate at the grain boundaries of the $BaTiO_3$ grains. The presence of such fine Ni particles prohibits the growth of $BaTO_3$ grains; the size of the matrix grains is thus small.

Figure 4 shows the lattice parameters of Ni-doped $BaTiO_3$ as a function of Ni content. The ratio of c over a is also shown in the figure. The c/a ratio reaches a constant value when the Ni content is higher than 0.52 mol%, indicating that the solubility of Ni in $BaTiO_3$ under the present experimental set-up is 5,200 ppm.

Since the Ni inclusions are relatively small, as demonstrated in Fig. 3, atomic mapping of the locations of these inclusions is conducted first(see Fig. 5a). The EPMA spot analysis is then conducted every one micrometer along a straight line across the Ni particles. The probing of EPMA-WDS is capable of collecting data up to a depth of about 1 μm from the specimen's surface; hence, the mapping probe size is larger than the actual size of the Ni inclusions. As mentioned in the experimental procedures, the EPMA-WDS data from five different probing lines were obtained from the polished surface. Figure 5b shows the EPMA-WDS result for the microstructure shown in Fig. 5a; the specimen used is 3.5 mol% Ni-doped $BaTiO_3$. In Fig. 5b, the plateau value shown in the middle part of the curve is taken as the solubility. In Fig. 5b, the solubility of Ni in $BaTiO_3$ is 5,600±770 ppm. The EPMA results for various specimens are shown in Table 2. From the Table, the average solubility of Ni in $BaTiO_3$ determined by the EPMA-WDS technique is 6,000±840 ppm.

Figures 6 and 7 show the relative permittivity and dissipation factor of the Ni-doped $BaTiO_3$ as a function of Ni content. The relative permittivity and dissipation factor of pure $BaTiO_3$ are high. A tiny amount of Ni doping (e.g.

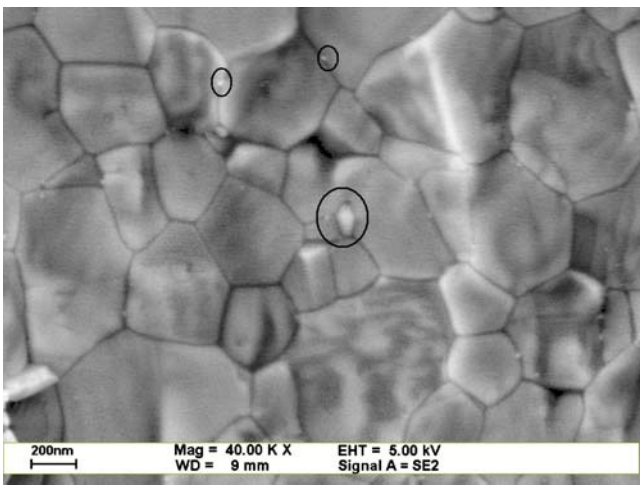

Fig. 3 Typical micrograph of 32 mol% Ni-doped $BaTiO_3$ specimen after sintering. Several Ni particles are *circled*

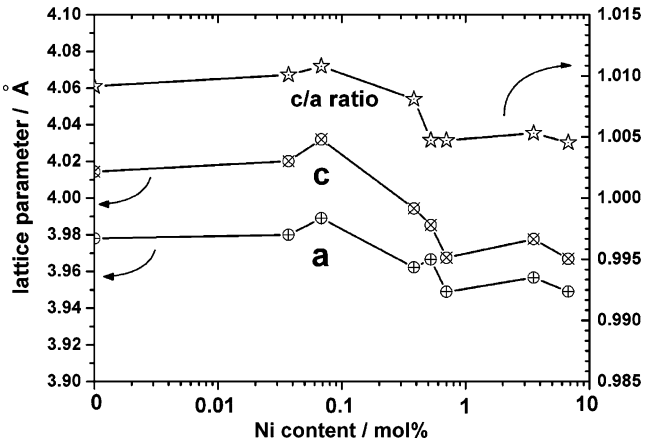

Fig. 4 Lattice parameters *c* and *a*, and *c*/*a* ratio for $BaTiO_3$ of the sintered Ni-doped $BaTiO_3$ specimens as function of Ni content

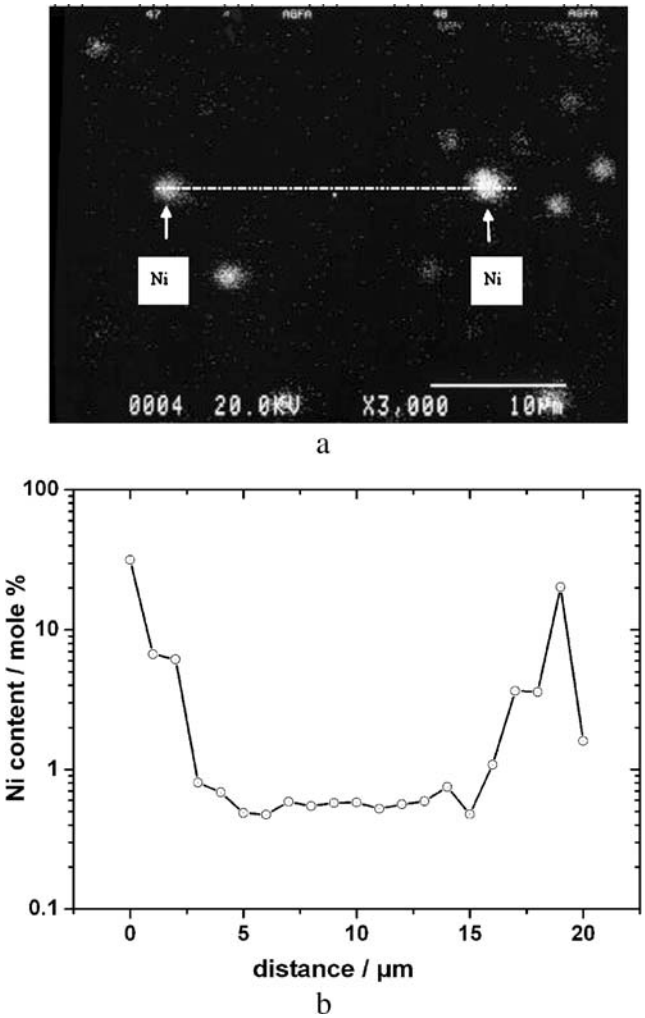

Fig. 5 Typical **a** Ni mapping **b** and corresponding EPMA-WDS result for a 3.5 mol% Ni-doped $BaTiO_3$ specimen

370 ppm) can reduce the relative permittivity and dissipation factor dramatically. The electrical resistivity of the Ni-doped $BaTiO_3$ is shown as a function of Ni content in Fig. 8. A tiny amount Ni doping can increase the electrical resistivity significantly.

4 Discussion

For the specimen shown in Fig. 1, there is 32 mol% of Ni in the starting Ni/$BaTiO_3$ powder mixture as determined by the ICP-AES technique. However, one should notice that only a very small amount of Ni is dissolved into $BaTiO_3$ in the form of Ni ion. Part of the Ni particles is oxidized after sintering in nitrogen, and part is still in their metallic form.

Table 2 Solubility of Ni in $BaTiO_3$ as determined by EPMA-WDS.

Ni content/mol%	Solubility/ppm
0.7	5,400±540
3.5	5,540±620
6.8	7,240±700

The solubility data obtained from the two techniques, XRD and EPMA, all indicate that an amount of 5,000–6,000 ppm of Ni is dissolved into $BaTiO_3$ after sintering at 1,330 °C for 2 h in nitrogen. The solubility of a dopant depends strongly on its charge and size. Though the valence states of Ni and Ba are the same, the ionic size of Ni (0.069 nm) is much smaller than that of Ba (0.161 nm), but close to that of Ti (0.0605 nm) [10]. The possibility of replacing Ti ions with Ni ions has been proposed by Tzing and Tuan [6]. Upon the replacement of Ti with Ni, the Ni solutes act as an acceptor to $BaTiO_3$.

Under the thermodynamic equilibrium condition, the decrease in oxygen partial pressure would promote the formation of oxygen vacancies, as shown in the following reaction [11, 12],

$$O_0 \rightarrow \frac{1}{2}O_2 + V_O^{\bullet\bullet} + 2e' \quad (1)$$

Based on the same reaction, the production of free electrons would decrease the electrical resistivity and increase consequently the dissipation factor (see Figs. 7 and 8). The solution of acceptor ions can also induce the formation of oxygen vacancies as demonstrated in the following reaction:

$$NiO \overset{BaTiO_3}{\rightarrow} Ni_{Ti}'' + 2V_O^{\bullet\bullet} + V_{BA}'' + O_0 \quad (2)$$

Based on Reaction (2), the solution of Ni acceptor can suppress Reaction (1). Hence, the amount of free electrons is reduced. Reaction (2) is confirmed by the increase in electrical resistivity of the Ni-doped $BaTiO_3$ (see Fig. 8).

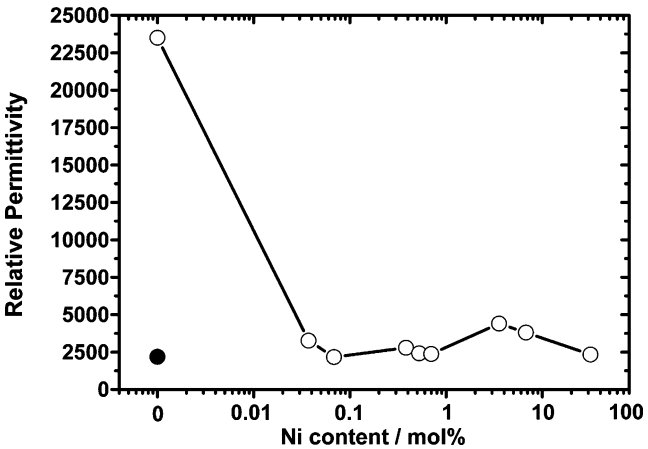

Fig. 6 Relative permittivity at room temperature of Ni-doped $BaTiO_3$ as function of Ni content. The value (solid circle) for the $BaTiO_3$ specimen prepared without pre-reduction is also shown for comparison

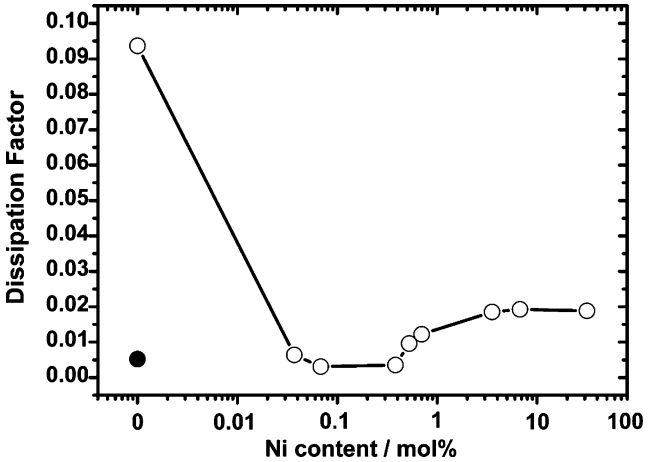

Fig. 7 Dissipation factor at room temperature of Ni-doped $BaTiO_3$ as function of Ni content. The value (*solid circle*) for the $BaTiO_3$ specimen prepared without pre-reduction is also shown for comparison

The electrical properties of the Ni-doped $BaTiO_3$ specimens validate the acceptor status of Ni in $BaTiO_3$.

Several recent studies indicated that the above thermodynamic equilibrium conditions are not attainable at low temperatures [13, 14]. The frozen-in metal vacancies are the major defects in these metastable $BaTiO_3$ specimens. The metastable states are also confirmed by the following comparison experiment. When the $BaTiO_3$ specimens are not pre-reduced at 800 °C in the N_2/H_2 gas mixture, their electrical properties show similar values to those of the Ni-doped $BaTiO_3$ specimens (see the solid circles in the Figs. 6, 7, and 8). It indicates that the pure $BaTiO_3$ specimens after reducing at 800 °C in N_2/H_2 are not fully re-oxidized after sintering at 1,330 °C for 2 h in N_2 (P_{O2}=1 Pa). The re-oxidation process has been investigated by Opitz et al recently [15]; their study also indicated that the re-oxidation of reduced $BaTiO_3$ is a time-consuming process.

There are two peaks in the EPMA-WDS intensity line (see Fig. 5b). These two peaks corresponds to the signal of the two Ni particles at both ends of the detection line (see Fig. 5a). The plateau at the middle of the intensity line is mainly resulted from the concentration of Ni in the $BaTiO_3$ grains. The height of the plateau is thus used as the solubility of Ni in $BaTiO_3$. The EPMA intensity line shown in Fig. 5b does not drop to zero within a detection length of 20 μm. In fact, most EPMA lines we have obtained did show the same trend, it indicates that the $BaTiO_3$ matrix is saturated with the Ni solutes. There are a large number of uniformly distributed fine Ni particles within the $BaTiO_3$ matrix, hence, the solution of Ni in $BaTiO_3$ can easily reach a saturated value. However, the electron probe can reach a depth of 1 μm from the surface. The electron probe can detect the amount of both Ni sloute and Ni particles under the surface. Though the Ni content in the Ni-doped $BaTiO_3$ specimens is small, since the size of Ni particles are very small, the chance of the electron probe to hit one Ni particles under the surface is still high. Therefore, the EPMA technique reported a slightly higher solubility. Furthermore, the technique also found that the solubility increases slightly with the increase of Ni content (see Table 2), it suggests that the value obtained from the EPMA technique can only be treated as the upper limit. The EPMA result for the $BaTiO_3$-0.7 mol% Ni specimen is therefore taken as the upper limit for the solubility of Ni in $BaTiO_3$, which is 5,400±540 ppm.

As long as the diffusion distance is concerned, the length of the plateau shown in the specific case shown in Fig. 5b is 11 μm. The Ni solutes within the plateau region may come from the two Ni particles at the ends of the detection line. They may also come from some nearby Ni particles under the surface, which could not be seen from the micrograph. In any case, it suggests that the diffusion distance is longer than the diameter of one electron probe, ~1.5 μm. Though the exact diffusion distance cannot be determined, a minimum value, 1 μm, can be estimated. Such diffusion distance is relatively long in terms of the dielectric thickness for multilayered structure. The present study demonstrates that the Ni solutes are readily dissolved into the dielectric matrix after co-firing. Nevertheless, the solution of Ni in $BaTiO_3$ is beneficial since the addition of Ni enhances the reduction resistance of $BaTiO_3$.

The oxidation of Ni to NiO takes place when the partial pressure of oxygen is higher than 0.1 Pa at 1,330 °C [16]. The oxygen partial pressure in the sintering atmosphere is 1 Pa, and therefore, partial oxidation of Ni after co-firing is expected. In the present study, Ni and NiO are co-existed within the Ni-doped $BaTiO_3$ specimens during co-firing. The effective oxygen partial pressure within the powder compacts during sintering is thus the same as the

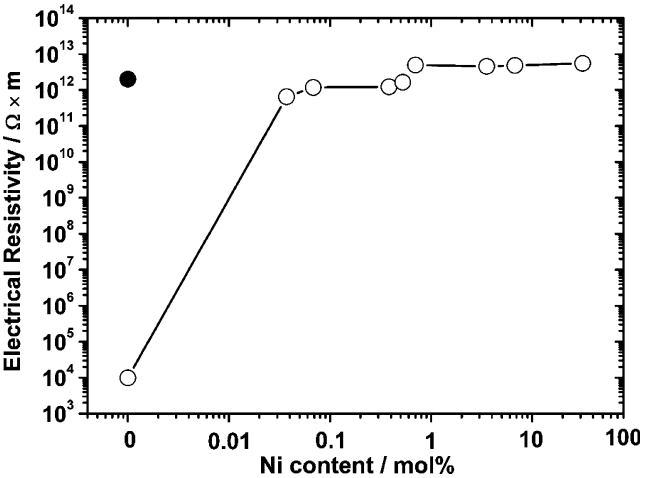

Fig. 8 Electrical resistivity at room temperature of Ni-doped $BaTiO_3$ as function of Ni content. The value (*solid circle*) for the $BaTiO_3$ specimen prepared without pre-reduction is also shown for comparison

equilibrium oxygen partial pressure for the reaction of Ni→NiO, which is 0.1 Pa [15].

Under the present experimental set-up, the oxygen partial pressure in the sintering atmosphere is higher than that used for the manufacturing of Ni-MLCC. The solubility of Ni ions decreases with the drop in oxygen partial pressure. Since the commercial Ni-MLCC components are sintered in an atmosphere with a much lower oxygen partial pressure [1]; the solubility of Ni in the dielectrics of Ni-MLCC is expected to be lower than the value reported in the present study.

5 Conclusions

Two experimental techniques, XRD and EPMA, are used in the present study to determine the solubility of Ni in $BaTiO_3$ under an oxygen partial pressure of 0.1 Pa. These two independent experimental techniques indicate that the upper limit of the solubility of Ni in $BaTiO_3$ is 5,400± 540 ppm at the temperature of 1,330 °C. The Ni solutes can diffuse a distance longer than 1 μm in pure $BaTiO_3$. The present study demonstrates that the nickel electrodes may dissolve into the $BaTiO_3$-based dielectrics during co-firing. The Ni solute acts as the acceptor to $BaTiO_3$, and their presence improves the reduction resistance of $BaTiO_3$-based dielectrics.

Acknowledgments The present study was supported by the National Science Council, Republic of China, through Contract No. NSC92-2216-E002-029. Valuable comments given by Prof. Jay Shieh, Dept. of Mater. Sci. & Eng., National Taiwan University, are highly appreciated. The technical help from Mr. Shiu-Sheng Chen is helpful.

References

1. H. Kishi, Y. Mizuno, H. Chazono, Jpn. J. Appl. Phys. **42**(1), 1 (2003)
2. P. Baxter, N.J. Hellicar, B. Lewis, J. Am. Ceram. Soc. **42**(10), 465 (1959)
3. I. Burn, G.H. Maher, J. Mater. Sci. **10**(2), 633 (1975)
4. H. Ihrig, J. Phys. C. Solid State Phys. **11**(5), 819 (1978)
5. H. Emoto, J. Hojo, J. Ceram. Soc. Jpn. Int. Ed. **100**(4), 553 (1992)
6. W.H. Tzing, W.H. Tuan, Ceram. Int. **25**(1), 69 (1999)
7. Z.L. Gui, Y.L. Wang, L.T. Li, Ceram. Int. **30**(5), 1275 (2004)
8. S.J. Shih, W.H. Tuan, J. Am. Ceram. Soc. **87**(3), 401 (2004)
9. B.D. Cullity, *Element of X-ray Diffraction*, 2nd edn. (Addison-Wesley, Reading, MA, 1978), p. 101
10. R.D. Shannon, Acta Crystallogr. A Found. Crystallogr. **32**(3), 751 (1976)
11. N-H. Chan, R.K. Sharma, D.M. Smyth, J. Am. Ceram. Soc. **65**(3), 167 (1982)
12. V. Bheemineni, E.K. Chang, M. Lal, M.P. Harmer, D.M. Smyth, J. Am. Ceram. Soc. **77**(12), 3173 (1994)
13. R. Moos, K.H. Hardtl, J. Am. Ceram. Soc. **78**(9), 2569 (1995)
14. Y. Tsur, C.A. Randall, J. Am. Ceram. Soc. **84**(9), 2147 (2001)
15. M.R. Opitz, K. Albertsen, J.J. Beeson, D.F. Hennings, J.L. Routbort, C.A. Randall, J. Am. Ceram. Soc. **86**(11), 1879 (2003)
16. O. Kubaschewski, E.L.L. Evans, C.B. Alcock, *Metallurgical Thermochemistry* (Pergamon, Oxford, 1967), p. 426